Evidence of Robust Half-metallicity in Strained Manganite Films

Gian Marco Pierantozzi,[*,†] Giovanni Vinai,*[*,†] Aleksandr Yu. Petrov,[†] Alessandro De Vita,[§] Federico Motti,[†,§,] Vincent Polewczyk,[†] Debashis Mondal,[†] Tommaso Pincelli,[†] Riccardo Cucini,[†] Chiara Bigi,[†] Ivana Vobornik,[†] Jun Fujii,[†] Piero Torelli,[†] Francesco Offi,[○] Giorgio Rossi,[†,§] Giancarlo Panaccione,[†] and Francesco Borgatti[⊥]*

[†] Istituto Officina dei Materiali (IOM)-CNR, Laboratorio TASC, Area Science Park, S.S. 14 km 163.5, Trieste I-34149, Italy

[§] Dipartimento di Fisica, Università di Milano, via Celoria 16, 20133 Milano, Italy

[○] Dipartimento di Scienze, Università degli Studi Roma Tre, Via della Vasca Navale 84, 00146 Roma, Italy

[⊥] CNR-ISMN, via Gobetti 101, Bologna, Italy

KEYWORDS

half-metal, manganites, spin polarization, double-exchange, phase separation

ABSTRACT

We investigated the relationship between ferromagnetism and metallicity in strained $La_{0.67}Ca_{0.33}MnO_3$ films grown on lattice mismatched $NdGaO_3(001)$, by means of spectroscopic techniques directly sensitive to the ferromagnetic state, to the band structure and to the chemical state of the atoms. In this system the ferromagnetic-metallic (FMM) phase spatially coexists with an insulating one in most of the phase diagram. Firstly, the observation of an almost 100% spin polarization of the photoelectrons at Fermi level in the fundamental state provides a direct evidence of the half-metallicity of the FMM phase, a result which has been previously observed through direct probe of the valence band only on unstrained, phase homogeneous $La_{0.67}Sr_{0.33}MnO_3$. Secondly, the spin polarization results to be correlated with the occupancy at the Fermi level for all the investigated temperature regimes. These outcomes show that the half-metallic behaviour predicted by double-exchange model persists even in phase-separated manganites. Moreover, the correlation between metallicity and ferromagnetic alignment is confirmed by X-ray Magnetic Circular Dichroism, a more bulk-sensitive technique, allowing to explain transport properties in terms of the conduction through aligned FMM domains.

INTRODUCTION

The electronic, magnetic and transport properties of the mixed-valence manganite oxides with $R_{1-x}A_xMnO_3$ perovskite structure (R = rare earth ion, A = alkaline ion) are mainly governed by the electron states of the Mn and O ions that are involved into the double exchange (DE) mechanism.[1] In this mechanism, the hopping of e_g electrons from Mn^{3+} to Mn^{4+} via the O^{2-} p-orbital is favored when the spins of the two Mn ions are parallel, hence resulting in a metallic and ferromagnetic state with a net separation between the spin-up ($e_{g\uparrow}$, $t_{2g\uparrow}$) and spin-down ($e_{g\downarrow}$, $t_{2g\downarrow}$) levels originating from the 3*d* single-ion orbitals.[2–5] If the Hund splitting energy

between the spin-up and spin-down states is larger than the bandwidth, the material is expected to be half-metallic, hence providing 100% spin polarized electrons at the Fermi level.[6,7] The achievement of huge spin polarization in spintronic devices, such as spin-polarized tunnel junctions and spin valves, has largely stimulated the search for half-metallic materials.[8,9] However, direct evidence through spin-polarized photoemission spectroscopy of 100% spin polarization for mixed-valence perovskite manganites was only achieved for "optimally doped" $La_{1-x}Sr_xMnO_3$ (LSMO, x = 0.33),[10] and has been highly debated.[11,12] In addition, the propensity of the manganites for exhibiting coexistence of mixed phases involving the ferromagnetic metallic (FMM) and an insulating phase, the latter often accompanied by charge/orbital and/or antiferromagnetic order, tends to contrast the attainment of a pure half-metallic behavior.[13,14] The coexistence of phases in manganites has attracted much interest in connection with the colossal magnetoresistance effect[15] and especially because it might open the way to magneto-caloric applications[16,17] and to the optical control of the magnetic state.[18–20] Given the wide range of potential applications opened by the phase coexistence, it is important to verify whether the claimed half-metallic behaviour is maintained even in this context. To our knowledge, half-metallicity in such systems was previously reported only once, in the case of $(La_{2/3}Pr_{1/3})_{5/8}Ca_{3/8}MnO_3$ (LPCMO) thin films, through tunnel magnetoresistance measurements.[21]

In this work, we use *in-situ* spin-resolved photoemission spectroscopy to investigate the electronic structure of strained $La_{1-x}Ca_xMnO_3$ (LCMO) films epitaxially grown on /$NdGaO_3$(001) (NGO) and post-annealed in pure O_2 atmosphere[22]. The resistivity of the films presents a wide temperature-dependent hysteresis accordingly with the occurrence of mixed phase condition previously reported.[23–25] We provide firm experimental evidence of the half-metallic character for the FMM phase through probing directly the spin polarization of the electronic states near the Fermi energy. The spin polarization is close to 100% in the

fundamental state, whereas its strong reduction at 150 K is accompanied by the depletion of the electronic states at Fermi level and by the modification of the whole band structure, consistently with the transition from a regime dominated by the FMM phase to one dominated by an insulating phase. The direct link between ferromagnetism and metallicity is also confirmed by more bulk-sensitive techniques. Indeed, from temperature-dependent X-ray Magnetic Circular Dichroism (XMCD) measurements at the Mn $L_{2,3}$ absorption edges, supported by Magneto-Optic Kerr Effect (MOKE) analysis, we infer that the increase of the electrical resistivity with the temperature can be explained with the misalignment of the FMM regions (due to thermal fluctuations and/or increase of the relative distance) and that conduction takes place only through regions magnetically aligned along the same direction, as expected on the basis of DE mechanism.

METHODS

Sample Growth and Transport Measurements. Thin films of $La_{0.67}Ca_{0.33}MnO_3$ with optimal doping x = 0.33 were grown on top of (001) NGO substrates for different thicknesses ranging from 8 nm to 60 nm. The films were grown by molecular beam epitaxy in the growth facility of APE beamline[26] at the Elettra synchrotron. The substrate temperature during the growth was kept at 720°C and the O_2 pressure was kept constant around 10^{-6} mbar. The growth of the films was monitored in operando by RHEED oscillations. Afterwards, as-grown samples were annealed *ex situ* in 1 bar of O_2 atmosphere at 800°C, for different time depending on the film's thickness. It has been supposed[22] that the post-growth annealing improves the film morphology and restores the correct stoichiometry by filling the oxygen vacancies formed during the growth.

Transport measurements were performed with two probes, since resistivity was too high to use Van Der Pauw method. No magnetic field was applied during the transport measurements.

Spin-ARPES measurements. The Spin-ARPES measurements were carried at APE-LE beamline[27] with hν = 78 eV in linear polarization and at an incidence angle of 40°, in zero field. The spin polarization of the photoelectrons was measured by means of V-LEED apparatus. Before the Spin-ARPES measurements, the films were annealed once again in an ultra-high vacuum chamber in 10^{-5} mbar O_2 atmosphere at 350°C to remove surface contaminants. This further step in the sample preparation has negligible effect on the transport properties.

XAS and XMCD measurements. The x-ray absorption spectra were performed at APE-HE beamline[28] in total electron yield (TEY) mode, at an incidence angle of 45°. The XMCD measurements at Mn $L_{2,3}$ edge were calculated either from two absorption spectra with different circular polarization (right and left) without applying any magnetic field (i.e. the same experimental conditions of the transport and Spin-ARPES measurements), or by keeping fixed the light circular polarization and measuring the absorption intensity at each spectral point after application of a magnetic field pulse in the two opposite direction along the easy magnetic axis (the intensity of the magnetic field was large enough to magnetically saturate the sample).

MOKE measurements. Longitudinal MOKE measurements were performed in a UHV apparatus.[26] The laser wavelength was 405 nm. After defining the easy axis with rotational longitudinal MOKE at 77 K, hysteresis loops were measured along the easy axis while cooling and heating the sample.

RESULTS AND DISCUSSION

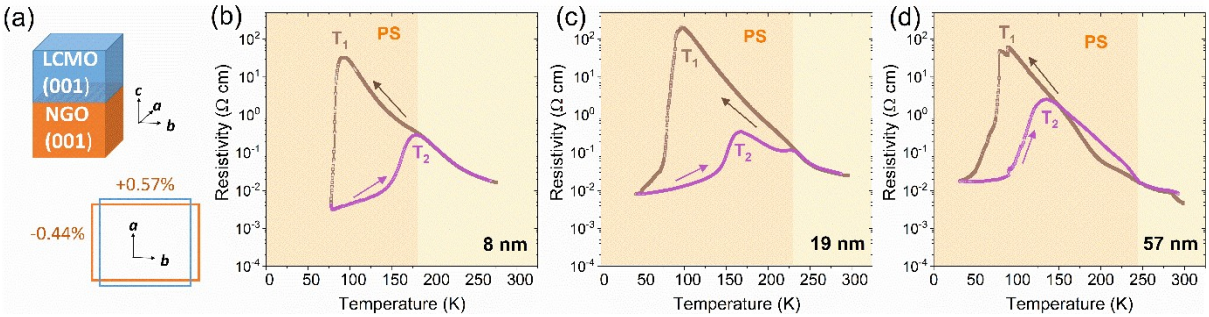

Figure 1. a) Schematic view of LCMO and NGO orthorhombic unit cells. (b-d) Transport measurements in zero-field cooling and warming for 8 nm (b), 20 nm (c) and 60 nm (d) LCMO films.

The electrical properties of the LCMO thin films with thickness among 8 and 60 nm, shown in **Figure 1,** are strictly related to the strain induced by the NGO(001) substrate, provided the subsequent annealing in O_2 atmosphere (see **Figure S6, Supporting Information**). The epitaxial matching with the NGO(001) substrate is sketched in **Figure 1**a. The NGO (001) substrate induces -0.44% (compressive) and +0.57% (tensile) strain respectively on the *a* and *b* axis of the LCMO orthorhombic unit cell. The consequent lattice distortion[29,30] produces important deviations from the bulk properties of LCMO in the "optimally doping" regime ($0.3 \leq x \leq 0.4$), namely a metallic ferromagnet with a well-defined Curie temperature (T_C) around 240 K.[31] A large hysteresis between the cooling and warming curves of the resistivity is observed for all the thicknesses, as displayed in **Figures 1**b-d. In particular, the temperature at which the sample makes the transition from insulating to metallic behavior along the decreasing temperature branch (T_1) is lower than the temperature at which the sample makes the opposite transition from metallic to insulating behavior along the increasing temperature branch (T_2).

The hysteresis in the resistivity was recognized since early works on manganites as a distinctive signature of a first-order phase transition hosting microscopic coexistence between metallic and insulating phases, strictly coupled to their respective magnetic/charge

ordering.[14,32–37] In the particular case of LCMO thin films grown on NGO(001), the phase separation (PS) scenario has been observed by magnetic force microscopy measurements.[24,38,39] This information helps to identify the PS regime (orange) in the panels of Figure 1 as the one where cooling and warming curves split, and the occurrence of a homogeneous insulating phase (yellow) above this point. It is worth to notice that the appearance of PS regime as inferred by transport curves, at about 160 K, 220 K and 240 K for the 8, 20 and 60 nm thick films, respectively, is close to the Curie temperature (T_C), as estimated from the persistence of magnetic hysteresis in MOKE measurements (see below for 8 nm film). The reduction of T_C at low thickness is expected due to the limitation of the spin-fluctuations.[40]

In order to investigate the magnetic nature of the FMM phase inside the PS scenario, we performed temperature-dependent Spin- and Angle-Resolved Photoemission (Spin-ARPES) measurements for the valence states of the 20 nm thick film. The results are summarized in **Figure 2**. The probing depth of these measurements was around 1 nm,[41] thus limiting the sensitivity to the surface region of the LCMO film. The spin- and momentum-integrated spectrum of the valence states is displayed in **Figure 2**a, measured first in the metallic regime at 20 K, then heating up to 150 K, i.e. close to T_2, and again cooling down to 20 K to verify the reproducibility. The difference between metallic (orange) and insulating (blue) regimes, as identified by transport measurement, is mirrored by the spectroscopic results, suggesting a good agreement between surface and bulk. Indeed, the density of states at the Fermi level (see the magnified spectra in the panel) shows a clear step edge at 20 K and 80 K, almost vanishing at 150 K, with a transfer of spectral weight to higher binding energies, and then recovered when cooling to 20 K again. Together with this, also the most intense peaks of the valence band in the region 3-7 eV have a reproducible trend with temperature, correlated to the height of the step edge at E_F. In the metallic regime, the two main peaks, attributed to oxygen states

hybridized with manganese ones[42–45] are well separated by a valley, as indicated by an orange arrow. By increasing the temperature, this valley tends to close, almost disappearing at 150 K. This behaviour is consistent with previous results measured on LSMO, showing a narrowing of the valence band in correspondence with an increasing insulating behaviour.[45] Finally, a satellite at 9 eV, marked with a blue arrow, appears only at 150 K and is then suppressed again when cooling to 20 K again. Its origin is difficult to assign, but its absence in DFT calculations[42] points towards a satellite due to many-body effects;[46] in any case, its intensity seems to be correlated to the amount of insulating phase. All these evident and reproducible modifications of the band structure passing from the low-temperature metallic regime to the insulating one prove that the FMM phase volume is strongly reduced in this transition.

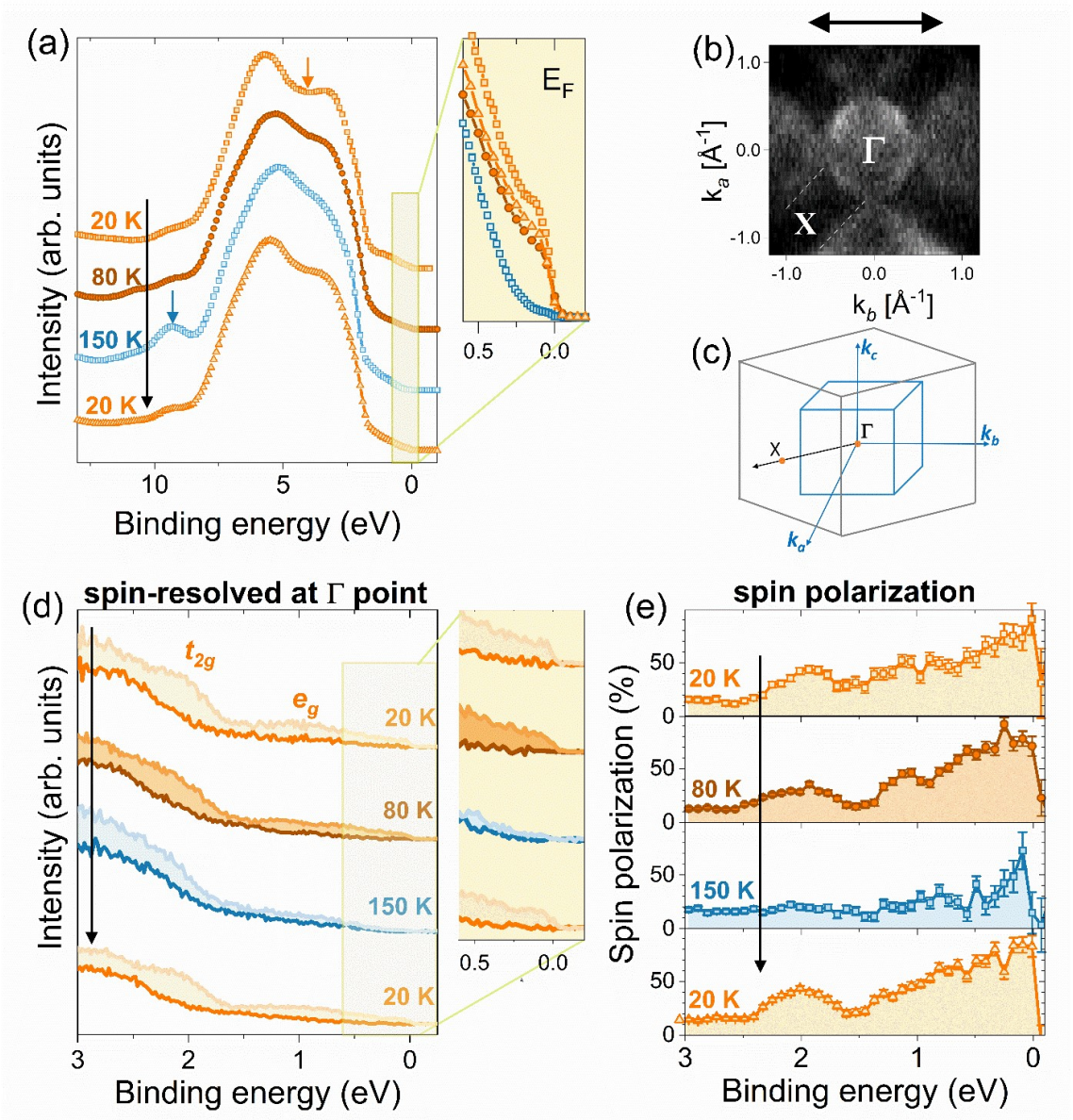

Figure 2. Angle-resolved photoemission spectra on 20 nm-thick LCMO film, acquired with hν = 78 eV linear polarization. a) Valence band momentum-integrated along k_b axis (at k_a = 0 A^{-1}) and zoom at Fermi edge along a thermal cycle (20 K→ 80 K → 150 K → 20 K). The spectra were normalized on the background at binding energy higher than 10 eV. b) Measured Fermi surface, at 20 K. Black is low intensity, white is high. c) Brillouin zone of a manganite system with orthorhombic unit cell, in light blue; the pseudo-cubic perovskite unit cell is drawn in gray (not in scale). The k_a and k_b axis of the light blue cell corresponds to the reference frame of panel b. d) Spin-resolved energy distribution curve at Γ from the Fermi level to -3 eV binding energy, measured along the same thermal cycle (the light curves represent majority spin and the darker ones minority spin). The measured intensities of the spin channels were calibrated by the experimental asymmetry (about 5% as measured from a reference Au surface) and divided by the Sherman function (0.3). The spin direction is indicated by the black arrow in (b). e) Spin polarization of the occupied electron states as resulting from the spectra in panel d (difference over sum).

The Fermi surface of the LCMO thin film (measured at 20 K, **Figure 2**b) shows an electron pocket located at the centre of the Brillouin zone, in agreement with previous results for LSMO.[12,47–49] We also recognize, highlighted by dashed lines, the border of the cuboids along Γ-X direction of the pseudo-cubic unit cell of the perovskite. The latter is indeed rotated by 45° with respect to orthorhombic unit cell along which k_a and k_b are defined, as depicted in **Figure 2**c.

In **Figure 2**d we report the spin resolved spectra at the investigated temperatures, measured at the Γ point, whereas **Figure 2**e shows the resulting spin polarization. The orientation of the spin probed in these measurements, indicated with a black arrow in **Figure 2**b, is along the *b* axis of the orthorhombic unit cell, corresponding to the easy magnetization axis according to MOKE measurements (see **Figure S1, Supporting Information**). Zero spin polarization was measured in the orthogonal in-plane direction (see **Figure S4, Supporting Information**). On the basis of previous theoretical calculations,[2,42] we identify the spectral terms attributed to t_{2g}- and e_g- derived states (the latter crossing the Fermi level), the two crystal-field splitted levels involved in the DE mechanism.[3] These two features are better distinguished in the difference spectra between the two spin channels, displayed in **Figure S3, Supporting Information**.

As highlighted in the inset of **Figure 2**d, at 20 K the spectrum of the majority states exhibits a finite intensity with a metallic cut-off at the Fermi energy, while the spectral intensity for the minority states becomes negligible more rapidly, indicating full depletion of the minority spin states. The resulting spin polarization at Fermi level is huge (around 90%), suggesting that the fundamental state is essentially half-metallic, and that both crystal-field split bands are spin polarized, as expected from DE model. The half-metallic condition in LCMO was previously reported only for unstrained optimally doped ferromagnetic films by scanning tunnelling microscopy,[50] whereas the only evidence in phase-separated manganites has been reported on

LPCMO films through tunnelling magnetoresistance.[21] More specifically, direct measurements of 100% valence band spin polarization, to which our data can be straightforwardly compared, has up to now only been reported in LSMO in homogeneous phase condition,[10] whose spin polarized spectrum lineshape is in striking agreement with our results. Considering this experimental evidence, we might reasonably argue that any further splitting of the Mn e_g and t_{2g} states promoted by the strain of the LCMO/NGO(001) films does not affect significantly the hopping of the free electrons in the FMM phase. The claim of half-metallicity is reinforced by the fact that similar spin polarization values were also obtained in points of the Fermi surface away from Γ (see **Figure S5, Supporting Information**).

The spin-resolved photoemission measurements as a function of the temperature (**Figure 2**d-e) show that the spin polarization of the FMM domains is correlated with the metallicity of the whole system. Warming the sample up to 80 K, i.e. still in the metallic regime, the spin polarization does not change, as well as both the electron occupancy at Fermi level and the band structure. At 150 K, i.e. close to T_2, the spin polarization on the e_g and t_{2g} derived features is considerably reduced, in combination with the spectral weight transfer to higher binding energy and the modification of the whole band structure. Assuming the mixed phase condition, these results suggest that at this temperature only a small part of the volume is still occupied by FMM domains, although they are still aligned along the same direction, at least partially (as proved by the residual spin polarization). It is likely that a further reduction of the volume occupied by this phase and the consequent increase of relative distance between the domains, along with the increase of thermal fluctuations, would reduce their alignment, thus explaining the incoming metal-to-insulator transition.

Summarizing the whole Spin-ARPES results, they are consistent with a PS scenario in which the FMM domains maintain the half-metallic behaviour typical of the bulk LCMO and explained by DE model, with the e_g–derived band crossing the Fermi level magnetically

coupled to the t_{2g}-derived one. The parallel alignment of the FMM domains and their size and relative distance as a function of the temperature determine the electron transport across the whole film.

To verify whether this interpretation can be extended from the surface region to the whole film, we performed XMCD measurements at Mn $L_{2,3}$ edges. Since the information depth of absorption spectroscopy in total electron yield is around 5 - 10 nm, we chose to study the 8 nm thick film, in order to probe most of the film thickness. The site and chemical sensitivity of this technique yield a measurement proportional to the absolute magnetic momentum of the elements in the sample, further resolving individual oxidation states. We are therefore able to exclude the spurious magnetization effects of non-stoichiometric Mn atoms at the surface. Furthermore, the dichroism measured without applied magnetic field, i.e. by reversing the light polarization after zero-field cooling the sample, allows to perform this investigation in the same conditions as transport measurement and Spin-ARPES experiment. We can compare the results with a second XMCD measurement, performed applying an external magnetic field of 25 mT, large enough to align all the FMM domains along the field direction, but small enough to avoid unbalancing the phase separation (see **Figure S2**, **Supporting Information**). This allows to quantify the volume fraction in the FMM phase at a certain temperature.

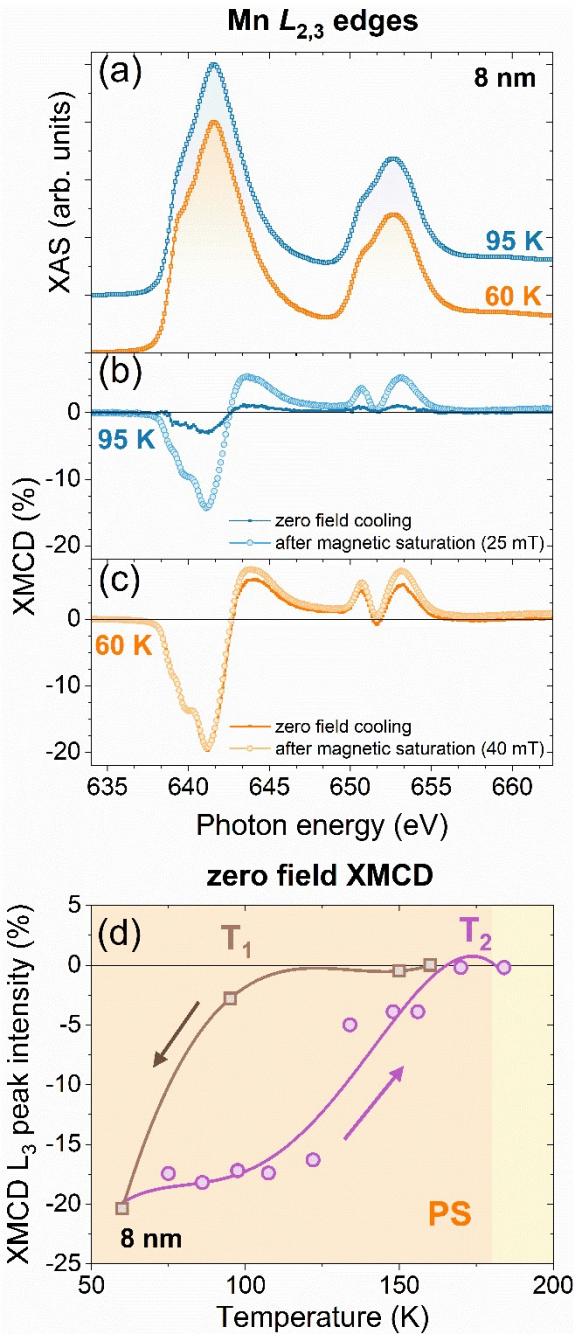

Figure 3. a) Absorption spectra at Mn $L_{2,3}$ edges of 8 nm thick film at 95 K (light blue) and 60 K (orange) in the cooling branch (sum of spectra acquired with opposite circularly polarized light). b) XMCD at 95 K, in zero field cooling and after magnetic saturation (magnetic field applied along the *b* axis of the sample) c) Same as b) at 60 K. d) Temperature-dependence of XCMD at Mn L_3 peak along a thermal cycle, measured in zero-field. The phase assignment is the same as Figure 1b, retrieved from resistivity measurements. The lines are guides to the eye. To obtain the XMCD peak intensities, the XAS spectra at opposite circular polarizations or opposite remanence magnetic fields were normalized to the L_3 edge intensity of the sum of the two spectra; then, the difference spectra were divided by 0.75·cos(45°) in order to account for both the 75% degree of circular polarization and the projection of the photon spin along the sample surface.

The sum of absorption spectra taken in the two opposite circular polarizations are shown in **Figure 3**a, measured at 95 K and 60 K (in both cases cooling from RT), e.g. across the insulator-to-metal transition temperature T_1. They present the typical lineshape as observed in mixed Mn^{3+}/Mn^{4+} valence manganites.[43,51–53] The resulting XMCD signals in zero-field, compared with those measured after magnetic saturation along the *b* axis, are displayed in **Figure 3**b and **Figure 3**c. At both temperatures, the shape of the dichroic signals is consistent with those obtained on other manganites,[51,52,54–57] including bulk LCMO,[53] proving that the magnetic signal comes from the manganese sites of the film, with valence 4+ and 3+, and not from any other contribution (for example 2+ valence[52,56,58]).

At 95 K (**Figure 3**b), i.e. around T_1, the temperature of the transition to the metallic regime, a maximum dichroism of 3% at L_3 peak is observed in zero-field, reaching 15% at remanence after magnetic saturation. This relatively large dichroic signal measured at remanence must be compared with 20-25% values observed in phase-homogeneous FMM systems,[43,51,54] implying the presence of a relevant volume fraction of the FMM phase. The much lower zero-field dichroism could then be the resulting average of misaligned FMM domains, which hinder electron transport from one to another and thus explain the high resistance measured in **Figure 1**b. Instead, at 60 K (**Figure 3**c), i.e. at $T<<T_1$, inside the metallic regime, the zero-field dichroism strongly increases, superimposing to the curve measured at remanence, proving an easier self-alignment of the various FMM domains along the same direction, in agreement with the strong decrease in resistivity at this temperature.

A general picture is obtained when following the zero-field XMCD temperature trend along both cooling and heating branches, shown in **Figure 3**d: along the cooling branch the dichroism increases when $T < T_1$, whereas in the warming direction it starts to decrease at higher temperatures (around 130 K), finally going to zero in correspondence of T_2. The XMCD data clearly evidence the direct link between magnetic and transport properties, suggesting that

the high resistivity phase arises from a magnetic disorder between FMM domains. However, this spectroscopic evidence does not allow disentangling the spatial dynamics of the domain evolution: XMCD results are compatible with a percolation of the FMM (insulating) phase in the cooling (warming) branch as previously posited through MFM measurement[24] (and as suggested by our Spin-ARPES results), but also with a scenario in which the shape and size of the two phases remain fixed as a function of temperature, as observed in another work of the same group.[38] Indeed, the conduction between two domains could also take place through thin insulating walls, provided that the decrease of thermal fluctuations favor their parallel alignment.[59–61]

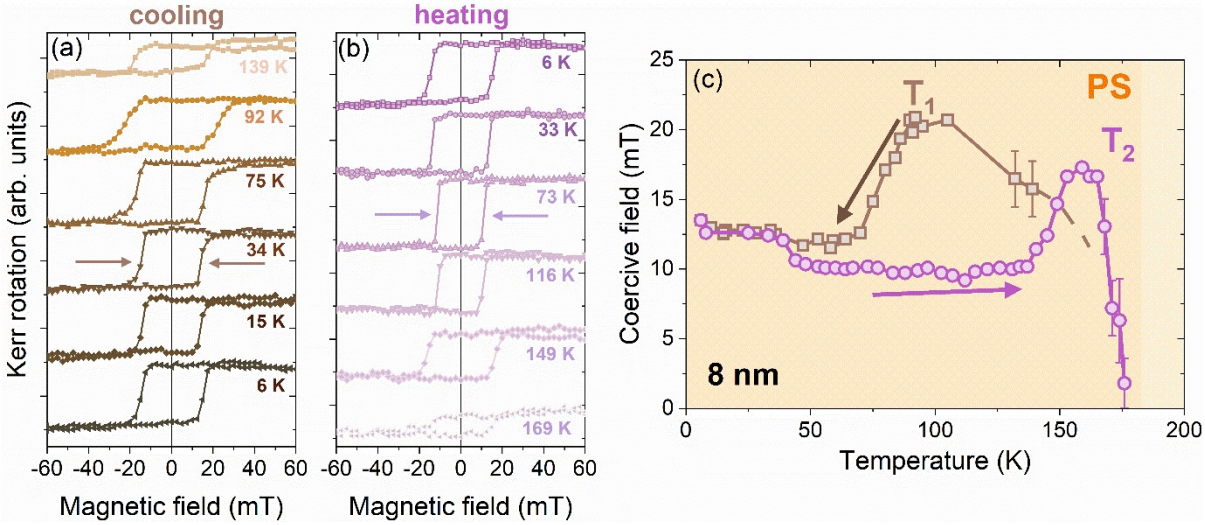

Figure 4. Selection of some MOKE measurements on 8 nm thick film, as a function of the magnetic field applied along *b* axis of sample at various temperatures during the sample cooling (a) and warming (b). (c) Trend of the coercive field, retrieved from hysteresis loop as half of the width of the loop taken at the point of intersection with magnetic field axis, as indicated by the arrows in (a) and (b). The phase assignment is the same as Figure 1b, retrieved from resistivity measurements.

Finally, the correlation of the metal-insulator transition temperature with the easy alignment of FMM domains is also confirmed by the temperature-dependence of the magnetic coercive field as measured by MOKE on the same 8 nm thick sample, shown in **Figure 4**, with

Figure 4a along the cooling process and **Figure 4**b along the warming one. The magnetic field was applied parallel to the in-plane easy axis (*b* axis of the orthorhombic unit cell), as verified by angular MOKE (see **Figure S1, Supporting Information**). The coercive field trend along the thermal cycle is displayed in **Figure 4**c. During the cooling, a local maximum of 20 mT is found in correspondence with T_1, followed by a decrease down to 12-13 mT in the metallic regime, similarly to what previously reported on thicker LCMO films[25]. In the warming sequence, the coercive field remains almost constant up to 130 K, where it starts again to increase. This hysteretic behaviour remarkably recalls the trends of both zero-field dichroism and electrical resistivity.

CONCLUSIONS

We investigated the relationship between ferromagnetism and metallicity on a strained LCMO film grown on lattice mismatched NGO(001), in which the FMM phase spatially coexists with an insulating one in most of the phase diagram, by means of spectroscopic techniques directly sensitive to the ferromagnetic state, the band structure and the chemical state of the atoms.

The most important outcome is the observation of an almost 100% spin polarization at Fermi level at 20 K, providing a direct evidence of the half-metallicity of the FMM phase in the fundamental state. The spin polarization remains constant increasing the temperature to 80 K and it is strongly reduced at 150 K; this drop is accompanied by an almost complete depletion of the states at Fermi level and a redistribution of spectral weight in the valence band, suggesting an increase of the volume occupied by the insulating phase at the expense of FMM regions.

These results prove that the half-metallic behaviour predicted by DE model and observed up to now only on unstrained, phase homogeneous LSMO, persists even in PS manganites, as long as the FMM phase remains dominant.

Moreover, the reduction of spin polarization of the outer electronic states at a temperature close to the metal-to-insulator transition implies that electrical conduction through the whole film is favoured until FMM regions are sufficiently close to each other so as to align easily along the same direction. The latter conclusion is confirmed by techniques able to probe all the film thickness: the trends both of the zero-field dichroism XMCD and of the value of the coercive field, which are both sensible to the easiness of alignment of magnetic domains, have a striking correspondence with the transport curves.

ASSOCIATED CONTENT

Supporting Information

The following files are available free of charge. Additional information on angular Kerr effect measurements on strained 8 nm film at 77 K, resistivity anisotropy and transport under magnetic field on strained 8 nm film, additional details on spin polarization, on the transport properties and XAS/XMCD measurements on "as-grown" film.

AUTHOR INFORMATION

Corresponding Authors

* Email: pierantozzi@iom.cnr.it

* Email: vinai@iom.cnr.it

Present Addresses

Federico Motti:

Laboratory for Mesoscopic Systems, Department of Materials, ETH Zurich, 8093 Zurich, Switzerland

Paul Scherrer Institute, 5232 Villigen PSI, Switzerland

Tommaso Pincelli:

Fritz-Haber Institute, Faradayweg 4-6, 14195 Berlin, Germany

Chiara Bigi:

SUPA, School of Physics and Astronomy, University of St. Andrews, St. Andrews KY16 9SS, United Kingdom

Author Contributions

G.M.P., G.P., G.V., T.P. and F.B. conceived the experiment. G.M.P., G.V. and F.B. wrote the paper with contributions from F.O., G.P. and A.Y.P.. All authors discussed the results, commented manuscript and prepared written contributions. A.Y.P. grew the films and characterized samples. G.M.P., G.V., A.D.V., F.M, V.P., D.M., F.O. and F.B. performed the experiments and analyzed the data.

Notes

The authors declare no competing financial interest.

ACKNOWLEDGMENT

This work has been partially performed in the framework of the Nanoscience Foundry and Fine Analysis (NFFA-MIUR Italy Progetti Internazionali) project.

G.M.P. thanks Pasquale Orgiani for fruitful discussion.

REFERENCES

(1) Salamon, M. B.; Jaime, M. The Physics of Manganites: Structure and Transport. *Rev. Mod. Phys.* **2001**, *73* (3), 583–628. https://doi.org/10.1103/RevModPhys.73.583.

(2) Pickett, W. E.; Singh, D. J. Electronic Structure and Half-Metallic Transport in the La1-XSrxMnO3 System. *Phys. Rev. B* **1996**, *53* (3), 1146–1160. https://doi.org/10.1103/PhysRevB.53.1146.

(3) Zener, C. Interaction between the D-Shells in the Transition Metals. II. Ferromagnetic

Compounds of Manganese with Perovskite Structure. *Phys. Rev.* **1951**, *82* (3), 403–405. https://doi.org/10.1103/PhysRev.82.403.

(4) Anderson, P. W.; Hasegawa, H. Considerations on Double Exchange. *Phys. Rev.* **1955**, *100* (2), 675–681. https://doi.org/10.1103/PhysRev.100.675.

(5) De Gennes, P. G. Effects of Double Exchange in Magnetic Crystals. *Phys. Rev.* **1960**, *118* (1), 141–154. https://doi.org/10.1103/PhysRev.118.141.

(6) De Groot, R. A.; Mueller, F. M.; Engen, P. G. V.; Buschow, K. H. J. New Class of Materials: Half-Metallic Ferromagnets. *Phys. Rev. Lett.* **1983**, *50* (25), 2024–2027. https://doi.org/10.1103/PhysRevLett.50.2024.

(7) Katsnelson, M. I.; Irkhin, V. Y.; Chioncel, L.; Lichtenstein, A. I.; De Groot, R. A. Half-Metallic Ferromagnets: From Band Structure to Many-Body Effects. *Rev. Mod. Phys.* **2008**, *80* (2), 315–378. https://doi.org/10.1103/RevModPhys.80.315.

(8) Bader, S. D.; Parkin, S. S. P. Spintronics. *Annu. Rev. Condens. Matter Phys.* **2010**, *1* (1), 71–88. https://doi.org/10.1146/annurev-conmatphys-070909-104123.

(9) Haghiri-Gosnet, A. M.; Arnal, T.; Soulimane, R.; Koubaa, M.; Renard, J. P. Spintronics: Perspectives for the Half-Metallic Oxides. *Phys. Status Solidi Appl. Res.* **2004**, *201* (7), 1392–1397. https://doi.org/10.1002/pssa.200304403.

(10) Park, J. H.; Vescovo, E.; Kim, H. J.; Kwon, C.; Ramesh, R.; Venkatesan, T. Direct Evidence for a Half-Metallic Ferromagnet. *Nature* **1998**, *392* (6678), 794–796. https://doi.org/10.1038/33883.

(11) Nadgorny, B.; Mazin, I. I.; Osofsky, M.; Soulen, R. J.; Broussard, P.; Stroud, R. M.; Singh, D. J.; Harris, V. G.; Arsenov, A.; Mukovskii, Y. Origin of High Transport Spin

Polarization in La0.7Sr0.3MnO3: Direct Evidence for Minority Spin States. *Phys. Rev. B* **2001**, *63* (18), 1844331–1844335. https://doi.org/10.1103/physrevb.63.184433.

(12) Sun, Z.; Wang, Q.; Douglas, J. F.; Lin, H.; Sahrakorpi, S.; Barbiellini, B.; Markiewicz, R. S.; Bansil, A.; Fedorov, A. V.; Rotenberg, E.; Zheng, H.; Mitchell, J. F.; Dessau, D. S. Minority-Spin T2g States and the Degree of Spin Polarization in Ferromagnetic Metallic La2-2x Sr1+2x Mn2O 7 (x = 0.38). *Sci. Rep.* **2013**, *3* (1), 3167. https://doi.org/10.1038/srep03167.

(13) Millis, A. J. Lattice Effects in Magnetoresistive Manganese Perovskites. *Nature* **1998**, *392* (6672), 147–150. https://doi.org/10.1038/32348.

(14) Tokura, Y. Critical Features of Colossal Magnetoresistive Manganites. *Reports Prog. Phys.* **2006**, *69* (3), 797–851. https://doi.org/10.1088/0034-4885/69/3/R06.

(15) Dagotto, E.; Hotta, T.; Moreo, A. Colossal Magnetoresistant Materials: The Key Role of Phase Separation. *Phys. Rep.* **2001**, *344* (1–3), 1–153. https://doi.org/10.1016/S0370-1573(00)00121-6.

(16) Moya, X.; Hueso, L. E.; Maccherozzi, F.; Tovstolytkin, A. I.; Podyalovskii, D. I.; Ducati, C.; Phillips, L. C.; Ghidini, M.; Hovorka, O.; Berger, A.; Vickers, M. E.; Defay, E.; Dhesi, S. S.; Mathur, N. D. Giant and Reversible Extrinsic Magnetocaloric Effects in La 0.7 Ca 0.3 MnO 3 Films Due to Strain. *Nat. Mater.* **2013**, *12* (1), 52–58. https://doi.org/10.1038/nmat3463.

(17) Bingham, N. S.; Suszka, A. K.; Vaz, C. A. F.; Kim, H.; Heyderman, L. J. Interfacial Room Temperature Magnetism and Enhanced Magnetocaloric Effect in Strained La0.66Ca0.34MnO3/BaTiO3 Heterostructures. *Phys. Rev. B* **2017**, *96* (2), 24419. https://doi.org/10.1103/PhysRevB.96.024419.

(18) Zhang, J.; Tan, X.; Liu, M.; Teitelbaum, S. W.; Post, K. W.; Jin, F.; Nelson, K. A.; Basov, D. N.; Wu, W.; Averitt, R. D. Cooperative Photoinduced Metastable Phase Control in Strained Manganite Films. *Nat. Mater.* **2016**, *15* (9), 956–960. https://doi.org/10.1038/nmat4695.

(19) Langner, M. C.; Zhou, S.; Coslovich, G.; Chuang, Y. D.; Zhu, Y.; Robinson, J. S.; Schlotter, W. F.; Turner, J. J.; Minitti, M. P.; Moore, R. G.; Lee, W. S.; Lu, D. H.; Doering, D.; Denes, P.; Tomioka, Y.; Tokura, Y.; Kaindl, R. A.; Schoenlein, R. W. Ultrafast X-Ray and Optical Signatures of Phase Competition and Separation Underlying the Photoinduced Metallic Phase in Pr1-XCaxMnO3. *Phys. Rev. B* **2015**, *92* (15), 155148. https://doi.org/10.1103/PhysRevB.92.155148.

(20) Teitelbaum, S. W.; Ofori-Okai, B. K.; Cheng, Y.-H.; Zhang, J.; Jin, F.; Wu, W.; Averitt, R. D.; Nelson, K. A. Dynamics of a Persistent Insulator-to-Metal Transition in Strained Manganite Films. *Phys. Rev. Lett.* **2019**, *123* (26), 267201. https://doi.org/10.1103/PhysRevLett.123.267201.

(21) Yang, W.; Shi, Q.; Miao, T.; Li, Q.; Cai, P.; Liu, H.; Lin, H.; Bai, Y.; Zhu, Y.; Yu, Y.; Deng, L.; Wang, W.; Yin, L.; Sun, D.; Zhang, X.-G.; Shen, J. Achieving Large and Nonvolatile Tunable Magnetoresistance in Organic Spin Valves Using Electronic Phase Separated Manganites. *Nat. Commun.* **2019**, *10* (1), 3877. https://doi.org/10.1038/s41467-019-11827-0.

(22) Wang, L. F.; Tan, X. L.; Chen, P. F.; Zhi, B. W.; Chen, B. B.; Huang, Z.; Gao, G. Y.; Wu, W. B. Annealing Assisted Substrate Coherency and High-Temperature Antiferromagnetic Insulating Transition in Epitaxial La0.67Ca 0.33MnO3/NdGaO3(001) Films. *AIP Adv.* **2013**, *3* (5), 52106. https://doi.org/10.1063/1.4804541.

(23) Huang, Z.; Wang, L.; Tan, X.; Chen, P.; Gao, G.; Wu, W. Phase Evolution and the Multiple Metal-Insulator Transitions in Epitaxially Shear-Strained La0.67Ca0.33MnO3/NdGaO 3 (001) Films. *J. Appl. Phys.* **2010**, *108* (8), 83912. https://doi.org/10.1063/1.3499650.

(24) Zhou, H.; Wang, L.; Hou, Y.; Huang, Z.; Lu, Q.; Wu, W. Evolution and Control of the Phase Competition Morphology in a Manganite Film. *Nat. Commun.* **2015**, *6* (1), 8980. https://doi.org/10.1038/ncomms9980.

(25) Jin, F.; Feng, Q.; Guo, Z.; Lan, D.; Chen, B.; Xu, H.; Wang, Z.; Wang, L.; Gao, G.; Chen, F.; Lu, Q.; Wu, W. Multilevel Control of the Metastable States in a Manganite Film. *J. Appl. Phys.* **2017**, *121* (24), 245304. https://doi.org/10.1063/1.4989974.

(26) Vinai, G.; Motti, F.; Petrov, A. Y.; Polewczyk, V.; Bonanni, V.; Edla, R.; Gobaut, B.; Fujii, J.; Suran, F.; Benedetti, D.; Salvador, F.; Fondacaro, A.; Rossi, G.; Panaccione, G.; Davidson, B. A.; Torelli, P. An Integrated Ultra-High Vacuum Apparatus for Growth and in Situ Characterization of Complex Materials. *Rev. Sci. Instrum.* **2020**, *91* (8), 85109. https://doi.org/10.1063/5.0005302.

(27) Bigi, C.; Das, P. K.; Benedetti, D.; Salvador, F.; Krizmancic, D.; Sergo, R.; Martin, A.; Panaccione, G.; Rossi, G.; Fujii, J.; Vobornik, I. Very Efficient Spin Polarization Analysis (VESPA): New Exchange Scattering-Based Setup for Spin-Resolved ARPES at APE-NFFA Beamline at Elettra. *J. Synchrotron Radiat.* **2017**, *24* (4), 750–756. https://doi.org/10.1107/S1600577517006907.

(28) Panaccione, G.; Vobornik, I.; Fujii, J.; Krizmancic, D.; Annese, E.; Giovanelli, L.; Maccherozzi, F.; Salvador, F.; De Luisa, A.; Benedetti, D.; Gruden, A.; Bertoch, P.; Polack, F.; Cocco, D.; Sostero, G.; Diviacco, B.; Hochstrasser, M.; Maier, U.; Pescia,

D.; Back, C. H.; Greber, T.; Osterwalder, J.; Galaktionov, M.; Sancrotti, M.; Rossi, G. Advanced Photoelectric Effect Experiment Beamline at Elettra: A Surface Science Laboratory Coupled with Synchrotron Radiation. *Rev. Sci. Instrum.* **2009**, *80* (4), 43105. https://doi.org/10.1063/1.3119364.

(29) Huang, Z.; Wang, L. F.; Chen, P. F.; Gao, G. Y.; Tan, X. L.; Zhi, B. W.; Xuan, X. F.; Wu, W. B. Tuning the Ground State of La 0.67Ca 0.33MnO 3 Films via Coherent Growth on Orthorhombic NdGaO 3 Substrates with Different Orientations. *Phys. Rev. B* **2012**, *86* (1), 14410. https://doi.org/10.1103/PhysRevB.86.014410.

(30) Jin, F.; Gu, M.; Ma, C.; Guo, E. J.; Zhu, J.; Qu, L.; Zhang, Z.; Zhang, K.; Xu, L.; Chen, B.; Chen, F.; Gao, G.; Rondinelli, J. M.; Wu, W. Uniaxial Strain-Controlled Ground States in Manganite Films. *Nano Lett.* **2020**, *20* (2), 1131–1140. https://doi.org/10.1021/acs.nanolett.9b04506.

(31) Schiffer, P.; Ramirez, A. P.; Bao, W.; Cheong, S. W. Low Temperature Magnetoresistance and the Magnetic Phase Diagram of La1-XCaxMnO3. *Phys. Rev. Lett.* **1995**, *75* (18), 3336–3339. https://doi.org/10.1103/PhysRevLett.75.3336.

(32) Uehara, M.; Mori, S.; Chen, C. H.; Cheong, S. W. Percolative Phase Separation Underlies Colossal Magnetoresistance in Mixed-Valent Manganites. *Nature* **1999**, *399* (6736), 560–563. https://doi.org/10.1038/21142.

(33) Zhang, L.; Israel, C.; Biswas, A.; Greene, R. L.; De Lozanne, A. Direct Observation of Percolation in a Manganite Thin Film. *Science (80-.).* **2002**, *298* (5594), 805–807. https://doi.org/10.1126/science.1077346.

(34) Lee, H. J.; Kim, K. H.; Kim, M. W.; Noh, T. W.; Kim, B. G.; Koo, T. Y.; Cheong, S. W.; Wang, Y. J.; Wei, X. Optical Evidence of Multiphase Coexistence in Single

Crystalline. *Phys. Rev. B* **2002**, *65* (11), 115118. https://doi.org/10.1103/PhysRevB.65.115118.

(35) Kiryukhin, V.; Kim, B. G.; Podzorov, V.; Cheong, S. W.; Koo, T. Y.; Hill, J. P.; Moon, I.; Jeong, J. H. Multiphase Segregation Andmetal-Insulator Transition in Single Crystal La5/8−yPryCa3/8MnO3. *Phys. Rev. B* **2001**, *63* (2), 24420. https://doi.org/10.1103/PhysRevB.63.024420.

(36) García-Muñoz, J. L.; Collado, A.; Aranda, M. A. G.; Ritter, C. Multilevel Hierarchy of Phase Separation Processes in La 5/8-YPryCa3/8MnO3. *Phys. Rev. B* **2011**, *84* (2), 24425. https://doi.org/10.1103/PhysRevB.84.024425.

(37) Ward, T. Z.; Budai, J. D.; Gai, Z.; Tischler, J. Z.; Yin, L.; Shen, J. Elastically Driven Anisotropic Percolation in Electronic Phase-Separated Manganites. *Nat. Phys.* **2009**, *5* (12), 885–888. https://doi.org/10.1038/nphys1419.

(38) Feng, Q.; Jin, F.; Zhou, H.; Wang, L.; Meng, W.; Zhang, K.; Wang, J.; Zhang, J.; Hou, Y.; Lu, Q.; Wu, W. Induced Formation of Structural Domain Walls and Their Confinement on Phase Dynamics in Strained Manganite Thin Films. *Adv. Mater.* **2018**, *30* (52), 1805353. https://doi.org/10.1002/adma.201805353.

(39) McLeod, A. S.; Zhang, J.; Gu, M. Q.; Jin, F.; Zhang, G.; Post, K. W.; Zhao, X. G.; Millis, A. J.; Wu, W. B.; Rondinelli, J. M.; Averitt, R. D.; Basov, D. N. Multi-Messenger Nanoprobes of Hidden Magnetism in a Strained Manganite. *Nat. Mater.* **2020**, *19* (4), 397–404. https://doi.org/10.1038/s41563-019-0533-y.

(40) De Andrés, A.; Rubio, J.; Castro, G.; Taboada, S.; Martínez, J. L.; Colino, J. M. Structural and Magnetic Properties of Ultrathin Epitaxial La 0.7Ca0.3MnO3 Manganite Films: Strain versus Finite Size Effects. *Appl. Phys. Lett.* **2003**, *83* (4), 713–715.

https://doi.org/10.1063/1.1594838.

(41) Powell, C. J.; Jablonski, A. NIST Electron Inelastic Mean Free Path, Version 1.2, SRD 71. National Institute of Standards and Technology, Gatihersburg 2010.

(42) Picozzi, S.; Ma, C.; Yang, Z.; Bertacco, R.; Cantoni, M.; Cattoni, A.; Petti, D.; Brivio, S.; Ciccacci, F. Oxygen Vacancies and Induced Changes in the Electronic and Magnetic Structures of La0.66 Sr0.33 Mn O3: A Combined Ab Initio and Photoemission Study. *Phys. Rev. B* **2007**, *75* (9), 94418. https://doi.org/10.1103/PhysRevB.75.094418.

(43) Bertacco, R.; Tagliaferri, A.; Riva, M.; Signorini, L.; Cantoni, M.; Cattoni, A.; Ciccacci, F.; Davidson, B. A.; Maccherozzi, F.; Vobornik, I.; Panaccione, G. Surface Electronic and Magnetic Properties of La2/3 Sr1/3 MnO3 Thin Films with Extended Metallicity above the Curie Temperature. *Phys. Rev. B* **2008**, *78* (3), 35448. https://doi.org/10.1103/PhysRevB.78.035448.

(44) Horiba, K.; Chikamatsu, A.; Kumigashira, H.; Oshima, M.; Nakagawa, N.; Lippmaa, M.; Ono, K.; Kawasaki, M.; Koinuma, H. In Vacuo Photoemission Study of Atomically Controlled La1-x Srx Mn O3 Thin Films: Composition Dependence of the Electronic Structure. *Phys. Rev. B* **2005**, *71* (15), 155420. https://doi.org/10.1103/PhysRevB.71.155420.

(45) Schlueter, C.; Orgiani, P.; Lee, T. L.; Petrov, A. Y.; Galdi, A.; Davidson, B. A.; Zegenhagen, J.; Aruta, C. Evidence of Electronic Band Redistribution in La 0.65Sr 0.35MnO 3-δ by Hard x-Ray Photoelectron Spectroscopy. *Phys. Rev. B* **2012**, *86* (15), 155102. https://doi.org/10.1103/PhysRevB.86.155102.

(46) McIlroy, D.; Waldfried, C.; Zhang, J.; Choi, J. W.; Foong, F.; Liou, S.; Dowben, P. Comparison of the Temperature-Dependent Electronic Structure of the Perovskites).

Phys. Rev. B **1996**, *54* (24), 17438–17451. https://doi.org/10.1103/PhysRevB.54.17438.

(47) Mannella, N.; Yang, W. L.; Zhou, X. J.; Zheng, H.; Mitchell, J. F.; Zaanen, J.; Devereaux, T. P.; Nagaosa, N.; Hussain, Z.; Shen, Z. X. Nodal Quasiparticle in Pseudogapped Colossal Magnetoresistive Manganites. *Nature* **2005**, *438* (7067), 474–478. https://doi.org/10.1038/nature04273.

(48) Krempaský, J.; Strocov, V. N.; Patthey, L.; Willmott, P. R.; Herger, R.; Falub, M.; Blaha, P.; Hoesch, M.; Petrov, V.; Richter, M. C.; Heckmann, O.; Hricovini, K. Effects of Three-Dimensional Band Structure in Angle- and Spin-Resolved Photoemission from Half-Metallic ${\mathrm{La}}_{2⁄3}{\mathrm{Sr}}_{1⁄3}\mathrm{Mn}{\mathrm{O}}_{3}$. *Phys. Rev. B* **2008**, *77* (16), 165120. https://doi.org/10.1103/PhysRevB.77.165120.

(49) Lev, L. L.; Krempaský, J.; Staub, U.; Rogalev, V. A.; Schmitt, T.; Shi, M.; Blaha, P.; Mishchenko, A. S.; Veligzhanin, A. A.; Zubavichus, Y. V.; Tsetlin, M. B.; Volfová, H.; Braun, J.; Minár, J.; Strocov, V. N. Fermi Surface of Three-Dimensional La1-XSrxMnO3 Explored by Soft-X-Ray ARPES: Rhombohedral Lattice Distortion and Its Effect on Magnetoresistance. *Phys. Rev. Lett.* **2015**, *114* (23), 237601. https://doi.org/10.1103/PhysRevLett.114.237601.

(50) Wei, J. Y. T.; Yeh, N. C.; Vasquez, R. P.; Gupta, A. Tunneling Evidence of Half-Metallicity in Epitaxial Films of Ferromagnetic Perovskite Manganites and Ferrimagnetic Magnetite. *J. Appl. Phys.* **1998**, *83* (11), 7366–7368. https://doi.org/10.1063/1.367799.

(51) Stadler, S.; Idzerda, Y. U.; Chen, Z.; Ogale, S. B.; Venkatesan, T. The Magnetism of a Buried La0.7Sr0.3MnO3 Interface. *Appl. Phys. Lett.* **1999**, *75* (21), 3384–3386.

https://doi.org/10.1063/1.125359.

(52) De Jong, M. P.; Bergenti, I.; Dediu, V. A.; Fahlman, M.; Marsi, M.; Taliani, C. Evidence for Mn 2+ Ions at Surfaces of La 0. 7Sr 0.3MnO 3 Thin Films. *Phys. Rev. B* **2005**, *71* (1), 14434. https://doi.org/10.1103/PhysRevB.71.014434.

(53) Werner, R.; Raisch, C.; Ruosi, A.; Davidson, B. A.; Nagel, P.; Merz, M.; Schuppler, S.; Glaser, M.; Fujii, J.; Chassé, T.; Kleiner, R.; Koelle, D. YBa2 Cu3 O7 / La0.7 Ca 0.3 MnO3 Bilayers: Interface Coupling and Electric Transport Properties. *Phys. Rev. B* **2010**, *82* (22), 224509. https://doi.org/10.1103/PhysRevB.82.224509.

(54) Park, J. H.; Vescovo, E.; Kim, H. J.; Kwon, C.; Ramesh, R.; Venkatesan, T. Magnetic Properties at Surface Boundary of a Half-Metallic Ferromagnet La0.7Sr0.3MnO3. *Phys. Rev. Lett.* **1998**, *81* (9), 1953–1956. https://doi.org/10.1103/PhysRevLett.81.1953.

(55) Pincelli, T. Probing Electron Correlation Dynamics: A Multi-Techinque Study Applied to the Half-Metallic Oxide La1-XSrxMnO3, Università degli Studi di Milano, 2017.

(56) Pesquera, D.; Barla, A.; Wojcik, M.; Jedryka, E.; Bondino, F.; Magnano, E.; Nappini, S.; Gutiérrez, D.; Radaelli, G.; Herranz, G.; Sánchez, F.; Fontcuberta, J. Strain-Driven Orbital and Magnetic Orders and Phase Separation in Epitaxial Half-Doped Manganite Films for Tunneling Devices. *Phys. Rev. Appl.* **2016**, *6* (3), 34004. https://doi.org/10.1103/PhysRevApplied.6.034004.

(57) Bruno, F. Y.; Garcia-Barriocanal, J.; Varela, M.; Nemes, N. M.; Thakur, P.; Cezar, J. C.; Brookes, N. B.; Rivera-Calzada, A.; Garcia-Hernandez, M.; Leon, C.; Okamoto, S.; Pennycook, S. J.; Santamaria, J. Electronic and Magnetic Reconstructions in La0.7Sr 0.3MnO3/SrTiO3 Heterostructures: A Case of Enhanced Interlayer Coupling Controlled by the Interface. *Phys. Rev. Lett.* **2011**, *106* (14), 147205.

https://doi.org/10.1103/PhysRevLett.106.147205.

(58) Valencia, S.; Gaupp, A.; Gudat, W.; Abad, L.; Balcells, L.; Cavallaro, A.; Martínez, B.; Palomares, F. J. Mn Valence Instability in La2/3 Ca1/3 Mn O3 Thin Films. *Phys. Rev. B* **2006**, *73* (10), 104402. https://doi.org/10.1103/PhysRevB.73.104402.

(59) Hwang, H. Y.; Cheong, S. W.; Ong, N. P.; Batlogg, B. Spin-Polarized Intergrain Tunneling in La2/3Sr1/3MnO3. *Phys. Rev. Lett.* **1996**, *77* (10), 2041–2044. https://doi.org/10.1103/PhysRevLett.77.2041.

(60) Gupta, A. .; Gong, G. Q; Xiao, G.; Duncombe, P. R.; Leoceur, P.; Trouilloud, P.; Wang, Y. Y.; Dravid, V. P.; Sun, J. Z. . Grain-Boundary Effects on the Magnetoresistance Properties of Perovskite Manganite Films. *Phys. Rev. B* **1996**, *54* (22), R15629–R15632. https://doi.org/10.1103/PhysRevB.54.R15629.

(61) Klein, J.; Höfener, C.; Uhlenbruck, S.; Alff, L.; Büchner, B.; Gross, R. On the Nature of Grain Boundaries in the Colossal Magnetoresistance Manganites. *Europhys. Lett.* **1999**, *47* (3), 371–377. https://doi.org/10.1209/epl/i1999-00398-1.

(1) Salamon, M. B.; Jaime, M. The Physics of Manganites: Structure and Transport. *Rev. Mod. Phys.* **2001**, *73* (3), 583–628. https://doi.org/10.1103/RevModPhys.73.583.

(2) Pickett, W. E.; Singh, D. J. Electronic Structure and Half-Metallic Transport in the La1-XSrxMnO3 System. *Phys. Rev. B* **1996**, *53* (3), 1146–1160. https://doi.org/10.1103/PhysRevB.53.1146.

(3) Zener, C. Interaction between the D-Shells in the Transition Metals. II. Ferromagnetic Compounds of Manganese with Perovskite Structure. *Phys. Rev.* **1951**, *82* (3), 403–405. https://doi.org/10.1103/PhysRev.82.403.

(4) Anderson, P. W.; Hasegawa, H. Considerations on Double Exchange. *Phys. Rev.* **1955**, *100* (2), 675–681. https://doi.org/10.1103/PhysRev.100.675.

(5) De Gennes, P. G. Effects of Double Exchange in Magnetic Crystals. *Phys. Rev.* **1960**, *118* (1), 141–154. https://doi.org/10.1103/PhysRev.118.141.

(6) De Groot, R. A.; Mueller, F. M.; Engen, P. G. V.; Buschow, K. H. J. New Class of Materials: Half-Metallic Ferromagnets. *Phys. Rev. Lett.* **1983**, *50* (25), 2024–2027. https://doi.org/10.1103/PhysRevLett.50.2024.

(7) Katsnelson, M. I.; Irkhin, V. Y.; Chioncel, L.; Lichtenstein, A. I.; De Groot, R. A. Half-Metallic Ferromagnets: From Band Structure to Many-Body Effects. *Rev. Mod. Phys.* **2008**, *80* (2), 315–378. https://doi.org/10.1103/RevModPhys.80.315.

(8) Bader, S. D.; Parkin, S. S. P. Spintronics. *Annu. Rev. Condens. Matter Phys.* **2010**, *1* (1), 71–88. https://doi.org/10.1146/annurev-conmatphys-070909-104123.

(9) Haghiri-Gosnet, A. M.; Arnal, T.; Soulimane, R.; Koubaa, M.; Renard, J. P. Spintronics: Perspectives for the Half-Metallic Oxides. *Phys. Status Solidi Appl. Res.* **2004**, *201* (7), 1392–1397. https://doi.org/10.1002/pssa.200304403.

(10) Park, J. H.; Vescovo, E.; Kim, H. J.; Kwon, C.; Ramesh, R.; Venkatesan, T. Direct Evidence for a Half-Metallic Ferromagnet. *Nature* **1998**, *392* (6678), 794–796. https://doi.org/10.1038/33883.

(11) Nadgorny, B.; Mazin, I. I.; Osofsky, M.; Soulen, R. J.; Broussard, P.; Stroud, R. M.; Singh, D. J.; Harris, V. G.; Arsenov, A.; Mukovskii, Y. Origin of High Transport Spin Polarization in La0.7Sr0.3MnO3: Direct Evidence for Minority Spin States. *Phys. Rev. B* **2001**, *63* (18), 1844331–1844335. https://doi.org/10.1103/physrevb.63.184433.

(12) Sun, Z.; Wang, Q.; Douglas, J. F.; Lin, H.; Sahrakorpi, S.; Barbiellini, B.; Markiewicz, R. S.; Bansil, A.; Fedorov, A. V.; Rotenberg, E.; Zheng, H.; Mitchell, J. F.; Dessau, D. S. Minority-Spin T2g States and the Degree of Spin Polarization in Ferromagnetic Metallic La2-2x Sr1+2x Mn2O 7 (x = 0.38). *Sci. Rep.* **2013**, *3* (1), 3167. https://doi.org/10.1038/srep03167.

(13) Millis, A. J. Lattice Effects in Magnetoresistive Manganese Perovskites. *Nature* **1998**, *392* (6672), 147–150. https://doi.org/10.1038/32348.

(14) Tokura, Y. Critical Features of Colossal Magnetoresistive Manganites. *Reports Prog. Phys.* **2006**, *69* (3), 797–851. https://doi.org/10.1088/0034-4885/69/3/R06.

(15) Dagotto, E.; Hotta, T.; Moreo, A. Colossal Magnetoresistant Materials: The Key Role of Phase Separation. *Phys. Rep.* **2001**, *344* (1–3), 1–153. https://doi.org/10.1016/S0370-1573(00)00121-6.

(16) Moya, X.; Hueso, L. E.; Maccherozzi, F.; Tovstolytkin, A. I.; Podyalovskii, D. I.; Ducati, C.; Phillips, L. C.; Ghidini, M.; Hovorka, O.; Berger, A.; Vickers, M. E.; Defay, E.; Dhesi, S. S.; Mathur, N. D. Giant and Reversible Extrinsic Magnetocaloric Effects in La 0.7 Ca 0.3 MnO 3 Films Due to Strain. *Nat. Mater.* **2013**, *12* (1), 52–58. https://doi.org/10.1038/nmat3463.

(17) Bingham, N. S.; Suszka, A. K.; Vaz, C. A. F.; Kim, H.; Heyderman, L. J. Interfacial Room Temperature Magnetism and Enhanced Magnetocaloric Effect in Strained La0.66Ca0.34MnO3/BaTiO3 Heterostructures. *Phys. Rev. B* **2017**, *96* (2), 24419. https://doi.org/10.1103/PhysRevB.96.024419.

(18) Zhang, J.; Tan, X.; Liu, M.; Teitelbaum, S. W.; Post, K. W.; Jin, F.; Nelson, K. A.;

Basov, D. N.; Wu, W.; Averitt, R. D. Cooperative Photoinduced Metastable Phase Control in Strained Manganite Films. *Nat. Mater.* **2016**, *15* (9), 956–960. https://doi.org/10.1038/nmat4695.

(19) Langner, M. C.; Zhou, S.; Coslovich, G.; Chuang, Y. D.; Zhu, Y.; Robinson, J. S.; Schlotter, W. F.; Turner, J. J.; Minitti, M. P.; Moore, R. G.; Lee, W. S.; Lu, D. H.; Doering, D.; Denes, P.; Tomioka, Y.; Tokura, Y.; Kaindl, R. A.; Schoenlein, R. W. Ultrafast X-Ray and Optical Signatures of Phase Competition and Separation Underlying the Photoinduced Metallic Phase in Pr1-XCaxMnO3. *Phys. Rev. B* **2015**, *92* (15), 155148. https://doi.org/10.1103/PhysRevB.92.155148.

(20) Teitelbaum, S. W.; Ofori-Okai, B. K.; Cheng, Y.-H.; Zhang, J.; Jin, F.; Wu, W.; Averitt, R. D.; Nelson, K. A. Dynamics of a Persistent Insulator-to-Metal Transition in Strained Manganite Films. *Phys. Rev. Lett.* **2019**, *123* (26), 267201. https://doi.org/10.1103/PhysRevLett.123.267201.

(21) Yang, W.; Shi, Q.; Miao, T.; Li, Q.; Cai, P.; Liu, H.; Lin, H.; Bai, Y.; Zhu, Y.; Yu, Y.; Deng, L.; Wang, W.; Yin, L.; Sun, D.; Zhang, X.-G.; Shen, J. Achieving Large and Nonvolatile Tunable Magnetoresistance in Organic Spin Valves Using Electronic Phase Separated Manganites. *Nat. Commun.* **2019**, *10* (1), 3877. https://doi.org/10.1038/s41467-019-11827-0.

(22) Wang, L. F.; Tan, X. L.; Chen, P. F.; Zhi, B. W.; Chen, B. B.; Huang, Z.; Gao, G. Y.; Wu, W. B. Annealing Assisted Substrate Coherency and High-Temperature Antiferromagnetic Insulating Transition in Epitaxial La0.67Ca 0.33MnO3/NdGaO3(001) Films. *AIP Adv.* **2013**, *3* (5), 52106. https://doi.org/10.1063/1.4804541.

(23) Huang, Z.; Wang, L.; Tan, X.; Chen, P.; Gao, G.; Wu, W. Phase Evolution and the Multiple Metal-Insulator Transitions in Epitaxially Shear-Strained La0.67Ca0.33MnO3/NdGaO 3 (001) Films. *J. Appl. Phys.* **2010**, *108* (8), 83912. https://doi.org/10.1063/1.3499650.

(24) Zhou, H.; Wang, L.; Hou, Y.; Huang, Z.; Lu, Q.; Wu, W. Evolution and Control of the Phase Competition Morphology in a Manganite Film. *Nat. Commun.* **2015**, *6* (1), 8980. https://doi.org/10.1038/ncomms9980.

(25) Jin, F.; Feng, Q.; Guo, Z.; Lan, D.; Chen, B.; Xu, H.; Wang, Z.; Wang, L.; Gao, G.; Chen, F.; Lu, Q.; Wu, W. Multilevel Control of the Metastable States in a Manganite Film. *J. Appl. Phys.* **2017**, *121* (24), 245304. https://doi.org/10.1063/1.4989974.

(26) Vinai, G.; Motti, F.; Petrov, A. Y.; Polewczyk, V.; Bonanni, V.; Edla, R.; Gobaut, B.; Fujii, J.; Suran, F.; Benedetti, D.; Salvador, F.; Fondacaro, A.; Rossi, G.; Panaccione, G.; Davidson, B. A.; Torelli, P. An Integrated Ultra-High Vacuum Apparatus for Growth and in Situ Characterization of Complex Materials. *Rev. Sci. Instrum.* **2020**, *91* (8), 85109. https://doi.org/10.1063/5.0005302.

(27) Bigi, C.; Das, P. K.; Benedetti, D.; Salvador, F.; Krizmancic, D.; Sergo, R.; Martin, A.; Panaccione, G.; Rossi, G.; Fujii, J.; Vobornik, I. Very Efficient Spin Polarization Analysis (VESPA): New Exchange Scattering-Based Setup for Spin-Resolved ARPES at APE-NFFA Beamline at Elettra. *J. Synchrotron Radiat.* **2017**, *24* (4), 750–756.

https://doi.org/10.1107/S1600577517006907.

(28) Panaccione, G.; Vobornik, I.; Fujii, J.; Krizmancic, D.; Annese, E.; Giovanelli, L.; Maccherozzi, F.; Salvador, F.; De Luisa, A.; Benedetti, D.; Gruden, A.; Bertoch, P.; Polack, F.; Cocco, D.; Sostero, G.; Diviacco, B.; Hochstrasser, M.; Maier, U.; Pescia, D.; Back, C. H.; Greber, T.; Osterwalder, J.; Galaktionov, M.; Sancrotti, M.; Rossi, G. Advanced Photoelectric Effect Experiment Beamline at Elettra: A Surface Science Laboratory Coupled with Synchrotron Radiation. *Rev. Sci. Instrum.* **2009**, *80* (4), 43105. https://doi.org/10.1063/1.3119364.

(29) Huang, Z.; Wang, L. F.; Chen, P. F.; Gao, G. Y.; Tan, X. L.; Zhi, B. W.; Xuan, X. F.; Wu, W. B. Tuning the Ground State of La 0.67Ca 0.33MnO 3 Films via Coherent Growth on Orthorhombic NdGaO 3 Substrates with Different Orientations. *Phys. Rev. B* **2012**, *86* (1), 14410. https://doi.org/10.1103/PhysRevB.86.014410.

(30) Jin, F.; Gu, M.; Ma, C.; Guo, E. J.; Zhu, J.; Qu, L.; Zhang, Z.; Zhang, K.; Xu, L.; Chen, B.; Chen, F.; Gao, G.; Rondinelli, J. M.; Wu, W. Uniaxial Strain-Controlled Ground States in Manganite Films. *Nano Lett.* **2020**, *20* (2), 1131–1140. https://doi.org/10.1021/acs.nanolett.9b04506.

(31) Schiffer, P.; Ramirez, A. P.; Bao, W.; Cheong, S. W. Low Temperature Magnetoresistance and the Magnetic Phase Diagram of La1-XCaxMnO3. *Phys. Rev. Lett.* **1995**, *75* (18), 3336–3339. https://doi.org/10.1103/PhysRevLett.75.3336.

(32) Uehara, M.; Mori, S.; Chen, C. H.; Cheong, S. W. Percolative Phase Separation Underlies Colossal Magnetoresistance in Mixed-Valent Manganites. *Nature* **1999**, *399* (6736), 560–563. https://doi.org/10.1038/21142.

(33) Zhang, L.; Israel, C.; Biswas, A.; Greene, R. L.; De Lozanne, A. Direct Observation of Percolation in a Manganite Thin Film. *Science (80-.).* **2002**, *298* (5594), 805–807. https://doi.org/10.1126/science.1077346.

(34) Lee, H. J.; Kim, K. H.; Kim, M. W.; Noh, T. W.; Kim, B. G.; Koo, T. Y.; Cheong, S. W.; Wang, Y. J.; Wei, X. Optical Evidence of Multiphase Coexistence in Single Crystalline. *Phys. Rev. B* **2002**, *65* (11), 115118. https://doi.org/10.1103/PhysRevB.65.115118.

(35) Kiryukhin, V.; Kim, B. G.; Podzorov, V.; Cheong, S. W.; Koo, T. Y.; Hill, J. P.; Moon, I.; Jeong, J. H. Multiphase Segregation Andmetal-Insulator Transition in Single Crystal La5/8−yPryCa3/8MnO3. *Phys. Rev. B* **2001**, *63* (2), 24420. https://doi.org/10.1103/PhysRevB.63.024420.

(36) García-Muñoz, J. L.; Collado, A.; Aranda, M. A. G.; Ritter, C. Multilevel Hierarchy of Phase Separation Processes in La 5/8-YPryCa3/8MnO3. *Phys. Rev. B* **2011**, *84* (2), 24425. https://doi.org/10.1103/PhysRevB.84.024425.

(37) Ward, T. Z.; Budai, J. D.; Gai, Z.; Tischler, J. Z.; Yin, L.; Shen, J. Elastically Driven Anisotropic Percolation in Electronic Phase-Separated Manganites. *Nat. Phys.* **2009**, *5* (12), 885–888. https://doi.org/10.1038/nphys1419.

(38) Feng, Q.; Jin, F.; Zhou, H.; Wang, L.; Meng, W.; Zhang, K.; Wang, J.; Zhang, J.; Hou, Y.; Lu, Q.; Wu, W. Induced Formation of Structural Domain Walls and Their

Confinement on Phase Dynamics in Strained Manganite Thin Films. *Adv. Mater.* **2018**, *30* (52), 1805353. https://doi.org/10.1002/adma.201805353.

(39) McLeod, A. S.; Zhang, J.; Gu, M. Q.; Jin, F.; Zhang, G.; Post, K. W.; Zhao, X. G.; Millis, A. J.; Wu, W. B.; Rondinelli, J. M.; Averitt, R. D.; Basov, D. N. Multi-Messenger Nanoprobes of Hidden Magnetism in a Strained Manganite. *Nat. Mater.* **2020**, *19* (4), 397–404. https://doi.org/10.1038/s41563-019-0533-y.

(40) De Andrés, A.; Rubio, J.; Castro, G.; Taboada, S.; Martínez, J. L.; Colino, J. M. Structural and Magnetic Properties of Ultrathin Epitaxial La 0.7Ca0.3MnO3 Manganite Films: Strain versus Finite Size Effects. *Appl. Phys. Lett.* **2003**, *83* (4), 713–715. https://doi.org/10.1063/1.1594838.

(41) Powell, C. J.; Jablonski, A. NIST Electron Inelastic Mean Free Path, Version 1.2, SRD 71. National Institute of Standards and Technology, Gatihersburg 2010.

(42) Picozzi, S.; Ma, C.; Yang, Z.; Bertacco, R.; Cantoni, M.; Cattoni, A.; Petti, D.; Brivio, S.; Ciccacci, F. Oxygen Vacancies and Induced Changes in the Electronic and Magnetic Structures of La0.66 Sr0.33 Mn O3: A Combined Ab Initio and Photoemission Study. *Phys. Rev. B* **2007**, *75* (9), 94418. https://doi.org/10.1103/PhysRevB.75.094418.

(43) Bertacco, R.; Tagliaferri, A.; Riva, M.; Signorini, L.; Cantoni, M.; Cattoni, A.; Ciccacci, F.; Davidson, B. A.; Maccherozzi, F.; Vobornik, I.; Panaccione, G. Surface Electronic and Magnetic Properties of La2/3 Sr1/3 MnO3 Thin Films with Extended Metallicity above the Curie Temperature. *Phys. Rev. B* **2008**, *78* (3), 35448. https://doi.org/10.1103/PhysRevB.78.035448.

(44) Horiba, K.; Chikamatsu, A.; Kumigashira, H.; Oshima, M.; Nakagawa, N.; Lippmaa, M.; Ono, K.; Kawasaki, M.; Koinuma, H. In Vacuo Photoemission Study of Atomically Controlled La1-x Srx Mn O3 Thin Films: Composition Dependence of the Electronic Structure. *Phys. Rev. B* **2005**, *71* (15), 155420. https://doi.org/10.1103/PhysRevB.71.155420.

(45) Schlueter, C.; Orgiani, P.; Lee, T. L.; Petrov, A. Y.; Galdi, A.; Davidson, B. A.; Zegenhagen, J.; Aruta, C. Evidence of Electronic Band Redistribution in La 0.65Sr 0.35MnO 3-δ by Hard x-Ray Photoelectron Spectroscopy. *Phys. Rev. B* **2012**, *86* (15), 155102. https://doi.org/10.1103/PhysRevB.86.155102.

(46) McIlroy, D.; Waldfried, C.; Zhang, J.; Choi, J. W.; Foong, F.; Liou, S.; Dowben, P. Comparison of the Temperature-Dependent Electronic Structure of the Perovskites). *Phys. Rev. B* **1996**, *54* (24), 17438–17451. https://doi.org/10.1103/PhysRevB.54.17438.

(47) Mannella, N.; Yang, W. L.; Zhou, X. J.; Zheng, H.; Mitchell, J. F.; Zaanen, J.; Devereaux, T. P.; Nagaosa, N.; Hussain, Z.; Shen, Z. X. Nodal Quasiparticle in Pseudogapped Colossal Magnetoresistive Manganites. *Nature* **2005**, *438* (7067), 474–478. https://doi.org/10.1038/nature04273.

(48) Krempaský, J.; Strocov, V. N.; Patthey, L.; Willmott, P. R.; Herger, R.; Falub, M.; Blaha, P.; Hoesch, M.; Petrov, V.; Richter, M. C.; Heckmann, O.; Hricovini, K. Effects of Three-Dimensional Band Structure in Angle- and Spin-Resolved Photoemission from Half-Metallic

${\mathrm{La}}_{2⁄3}{\mathrm{Sr}}_{1⁄3}\mathrm{Mn}{\mathrm{O}}_{3}$. *Phys. Rev. B* **2008**, *77* (16), 165120. https://doi.org/10.1103/PhysRevB.77.165120.

(49) Lev, L. L.; Krempaský, J.; Staub, U.; Rogalev, V. A.; Schmitt, T.; Shi, M.; Blaha, P.; Mishchenko, A. S.; Veligzhanin, A. A.; Zubavichus, Y. V.; Tsetlin, M. B.; Volfová, H.; Braun, J.; Minár, J.; Strocov, V. N. Fermi Surface of Three-Dimensional La1-XSrxMnO3 Explored by Soft-X-Ray ARPES: Rhombohedral Lattice Distortion and Its Effect on Magnetoresistance. *Phys. Rev. Lett.* **2015**, *114* (23), 237601. https://doi.org/10.1103/PhysRevLett.114.237601.

(50) Wei, J. Y. T.; Yeh, N. C.; Vasquez, R. P.; Gupta, A. Tunneling Evidence of Half-Metallicity in Epitaxial Films of Ferromagnetic Perovskite Manganites and Ferrimagnetic Magnetite. *J. Appl. Phys.* **1998**, *83* (11), 7366–7368. https://doi.org/10.1063/1.367799.

(51) Stadler, S.; Idzerda, Y. U.; Chen, Z.; Ogale, S. B.; Venkatesan, T. The Magnetism of a Buried La0.7Sr0.3MnO3 Interface. *Appl. Phys. Lett.* **1999**, *75* (21), 3384–3386. https://doi.org/10.1063/1.125359.

(52) De Jong, M. P.; Bergenti, I.; Dediu, V. A.; Fahlman, M.; Marsi, M.; Taliani, C. Evidence for Mn 2+ Ions at Surfaces of La 0. 7Sr 0.3MnO 3 Thin Films. *Phys. Rev. B* **2005**, *71* (1), 14434. https://doi.org/10.1103/PhysRevB.71.014434.

(53) Werner, R.; Raisch, C.; Ruosi, A.; Davidson, B. A.; Nagel, P.; Merz, M.; Schuppler, S.; Glaser, M.; Fujii, J.; Chassé, T.; Kleiner, R.; Koelle, D. YBa2 Cu3 O7 / La0.7 Ca 0.3 MnO3 Bilayers: Interface Coupling and Electric Transport Properties. *Phys. Rev. B* **2010**, *82* (22), 224509. https://doi.org/10.1103/PhysRevB.82.224509.

(54) Park, J. H.; Vescovo, E.; Kim, H. J.; Kwon, C.; Ramesh, R.; Venkatesan, T. Magnetic Properties at Surface Boundary of a Half-Metallic Ferromagnet La0.7Sr0.3MnO3. *Phys. Rev. Lett.* **1998**, *81* (9), 1953–1956. https://doi.org/10.1103/PhysRevLett.81.1953.

(55) Pincelli, T. Probing Electron Correlation Dynamics: A Multi-Techinque Study Applied to the Half-Metallic Oxide La1-XSrxMnO3, Università degli Studi di Milano, 2017.

(56) Pesquera, D.; Barla, A.; Wojcik, M.; Jedryka, E.; Bondino, F.; Magnano, E.; Nappini, S.; Gutiérrez, D.; Radaelli, G.; Herranz, G.; Sánchez, F.; Fontcuberta, J. Strain-Driven Orbital and Magnetic Orders and Phase Separation in Epitaxial Half-Doped Manganite Films for Tunneling Devices. *Phys. Rev. Appl.* **2016**, *6* (3), 34004. https://doi.org/10.1103/PhysRevApplied.6.034004.

(57) Bruno, F. Y.; Garcia-Barriocanal, J.; Varela, M.; Nemes, N. M.; Thakur, P.; Cezar, J. C.; Brookes, N. B.; Rivera-Calzada, A.; Garcia-Hernandez, M.; Leon, C.; Okamoto, S.; Pennycook, S. J.; Santamaria, J. Electronic and Magnetic Reconstructions in La0.7Sr 0.3MnO3/SrTiO3 Heterostructures: A Case of Enhanced Interlayer Coupling Controlled by the Interface. *Phys. Rev. Lett.* **2011**, *106* (14), 147205. https://doi.org/10.1103/PhysRevLett.106.147205.

(58) Valencia, S.; Gaupp, A.; Gudat, W.; Abad, L.; Balcells, L.; Cavallaro, A.; Martínez, B.; Palomares, F. J. Mn Valence Instability in La2/3 Ca1/3 Mn O3 Thin Films. *Phys. Rev. B* **2006**, *73* (10), 104402. https://doi.org/10.1103/PhysRevB.73.104402.

(59) Hwang, H. Y.; Cheong, S. W.; Ong, N. P.; Batlogg, B. Spin-Polarized Intergrain Tunneling in La2/3Sr1/3MnO3. *Phys. Rev. Lett.* **1996**, *77* (10), 2041–2044. https://doi.org/10.1103/PhysRevLett.77.2041.

(60) Gupta, A. .; Gong, G. Q; Xiao, G.; Duncombe, P. R.; Leoceur, P.; Trouilloud, P.; Wang, Y. Y.; Dravid, V. P.; Sun, J. Z. . Grain-Boundary Effects on the Magnetoresistance Properties of Perovskite Manganite Films. *Phys. Rev. B* **1996**, *54* (22), R15629–R15632. https://doi.org/10.1103/PhysRevB.54.R15629.

(61) Klein, J.; Höfener, C.; Uhlenbruck, S.; Alff, L.; Büchner, B.; Gross, R. On the Nature of Grain Boundaries in the Colossal Magnetoresistance Manganites. *Europhys. Lett.* **1999**, *47* (3), 371–377. https://doi.org/10.1209/epl/i1999-00398-1.